



**HAL**  
open science

## Topographic control of hydrogen deposits at low to mid latitudes of Mars

W. C. Feldman, T. H. Prettyman, S. Maurice, S. Nelli, R. Elphic, H. O. Funsten, O. Gasnault, D. J. Lawrence, J. R. Murphy, R. L. Tokar, et al.

► **To cite this version:**

W. C. Feldman, T. H. Prettyman, S. Maurice, S. Nelli, R. Elphic, et al.. Topographic control of hydrogen deposits at low to mid latitudes of Mars. *Journal of Geophysical Research Space Physics*, 2005, issue A, in press. hal-00013102

**HAL Id: hal-00013102**

**<https://hal.science/hal-00013102v1>**

Submitted on 19 Feb 2021

**HAL** is a multi-disciplinary open access archive for the deposit and dissemination of scientific research documents, whether they are published or not. The documents may come from teaching and research institutions in France or abroad, or from public or private research centers.

L'archive ouverte pluridisciplinaire **HAL**, est destinée au dépôt et à la diffusion de documents scientifiques de niveau recherche, publiés ou non, émanant des établissements d'enseignement et de recherche français ou étrangers, des laboratoires publics ou privés.

## Topographic control of hydrogen deposits at low latitudes to midlatitudes of Mars

W. C. Feldman,<sup>1</sup> T. H. Prettyman,<sup>1</sup> S. Maurice,<sup>2</sup> S. Nelli,<sup>3</sup> R. Elphic,<sup>1</sup> H. O. Funsten,<sup>1</sup> O. Gasnault,<sup>2</sup> D. J. Lawrence,<sup>1</sup> J. R. Murphy,<sup>3</sup> R. L. Tokar,<sup>1</sup> and D. T. Vaniman<sup>1</sup>

Received 14 April 2004; revised 21 July 2005; accepted 10 August 2005; published 30 November 2005.

[1] Correlations between the longitudinal wave number two distribution of water-equivalent hydrogen (WEH) at low latitudes to midlatitudes of Mars with variations in topography, surface albedo, thermal inertia, regional dust storms, and atmospheric water vapor are explored to provide guidance in determining the mechanisms that recharge or maintain these WEH reservoirs. The closest match is with low thermal inertia coupled with orographic control of the present-day atmospheric circulation dynamics. The engine for the simulated longitudinal two-wave pattern (maxima in Arabia and Tharsis) is relatively cold nighttime surface temperatures and large-amplitude temperature inversions that concentrate water ice over these regions. Geologically recent precipitated water ice, by itself, is insufficient to account for the observed distribution of WEH. Retention of precipitate by hydratable minerals is necessary. While current research cannot presently identify the hydration mechanism for the WEH distribution (whether it be from a past obliquity, present climate conditions, or some convolution of both), this research suggests that current climatic conditions can sustain, if not emplace, the observed longitudinally constrained distribution of equatorial WEH.

**Citation:** Feldman, W. C., et al. (2005), Topographic control of hydrogen deposits at low latitudes to midlatitudes of Mars, *J. Geophys. Res.*, 110, E11009, doi:10.1029/2005JE002452.

### 1. Introduction

[2] Global surveys of hydrogen deposits on Mars have revealed three major reservoirs [Feldman *et al.*, 2002, 2004a; Boynton *et al.*, 2002; Mitrofanov *et al.*, 2002; Tokar *et al.*, 2002; Prettyman *et al.*, 2004]. The two most abundant reservoirs reside at high latitudes, poleward of about  $\pm 60^\circ$ . They contain sufficient water-equivalent hydrogen (WEH, as much as 50% to 70% by mass), to more than fill the pore spaces thought to be available in surface soils [Tokar *et al.*, 2002; Prettyman *et al.*, 2004].

[3] The third major WEH reservoir consists of significant upper regolith minimum mass water abundances of between 2% and 10% residing at low latitudes to midlatitudes of Mars [Feldman *et al.*, 2002, 2004a]. The most comprehensive models of surface and subsurface thermal conditions show that water ice should not be stable within about  $30^\circ$  of the equator [Farmer and Doms, 1979; Paige, 1992; Jakosky and Haberle, 1992; Mellon and Jakosky, 1993]. This prediction is contrary to observations if the WEH is in the form of water ice. Initial analyses of these deposits therefore assumed that the observed near-equatorial WEH deposits are in the form of hydrated minerals [Basilevsky *et al.*, 2003;

Feldman *et al.*, 2004b]. Nevertheless, previously buried water ice cannot be ruled out if that ice is covered by dry layers of regolith having sufficiently low permeability to effectively isolate the ice from the atmosphere [Clifford, 1998; Mischna *et al.*, 2003; Mischna and Richardson, 2005; Richardson *et al.*, 2003; Feldman *et al.*, 2004c].

[4] In order to explore the factors that control low-latitude water distribution, the pattern of WEH deposits has been compared with that of many known surface features, such as elevation, albedo, rock abundance, atmospheric water vapor density, temperature, and thermal inertia [Feldman *et al.*, 2003; Jakosky *et al.*, 2005]. No global match was found. Nevertheless, regional correlations show promise of providing insight into potential factors that may contribute to the observed WEH distribution.

[5] For example, the correlation between WEH [Feldman *et al.*, 2004a] and the visible albedo [Christensen *et al.*, 2001], shown in the top two plots of Figure 1 shows that there appears to be no obvious correlation [Feldman *et al.*, 2003; Jakosky *et al.*, 2005]. Whereas the albedo is high over northern Arabia where WEH is high (centered on  $20^\circ\text{N}$  latitude,  $25^\circ\text{E}$  longitude), it switches sharply to a low albedo just south of the equator in Terra Sabaea where WEH remains high. This fact is demonstrated graphically in Figure 2 using meridional cuts through both WEH and albedo at east longitudes of  $-3^\circ$  and  $+15^\circ$ . Here, both the albedo and WEH are high in the neighborhood of  $+20^\circ$  latitude, the WEH is high and the albedo is low near  $-10^\circ$  latitude, and the albedo is high and WEH is low near  $-50^\circ$  latitude. Also, while the albedo is high over the meridional lane of high WEH

<sup>1</sup>Los Alamos National Laboratory, Los Alamos, New Mexico, USA.

<sup>2</sup>Centre d'Etude Spatiale des Rayonnements, Toulouse, France.

<sup>3</sup>Department of Astronomy, New Mexico State University, Las Cruces, New Mexico, USA.

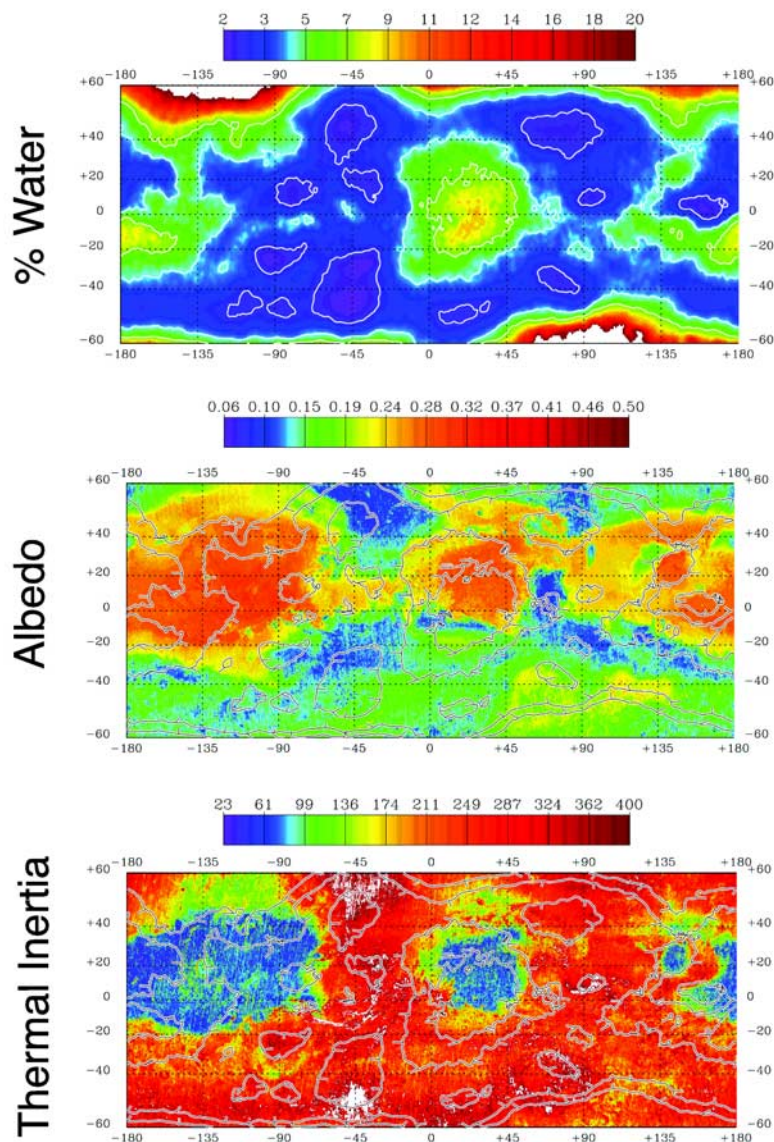


**Figure 1.** Maps of WEH, albedo, and thermal inertia in cylindrical projection between  $\pm 60^\circ$ . Contours of WEH corresponding to 3%, 5%, and 7% are overlain on all three maps.

that connects the equator to the northern high-WEH reservoir just west of the Tharsis province (centered at about  $140^\circ$ W longitude), the albedo remains high over a large area both east and west of this lane where WEH is low.

[6] A partial correlation that does encourage a deeper analysis is evident in a comparison between the distribution of WEH and thermal inertia [Mellon *et al.*, 2002], shown in the top and bottom plots of Figure 1. Both show a similar longitudinal wave number two distribution between  $\pm 60^\circ$  latitude. This correlation is significant because the coldest near-surface temperatures are associated with locations of lowest surface thermal inertia, which should also be places where water ice and hydrous minerals would be most stable.

[7] Under the assumption that the observed WEH is in the form of water ice, Jakosky *et al.* [2005] used the lack of a global correlation between WEH and any known surface

feature to search for a time-dependent cause by postulating a recent disappearance of the present  $\text{CO}_2$  veneer that covers the residual south polar water ice cap. Such an exposure would then lead to an increase in the water vapor content of the atmosphere that may be sufficiently large to stabilize near-equatorial water ice just below the surface, at least temporarily. According to this hypothesis, the  $\text{CO}_2$  veneer has since returned, thereby reducing the atmospheric water content to the point where the putative temporary subsurface WEH deposits are no longer stable. At the present time, this water ice then should be slowly evaporating with timescale less than about  $10^4$  years [Mellon *et al.*, 2004; Mischna and Richardson, 2005] although a remnant from the earlier, atmospheric water-rich epoch may still be present.

[8] If on the other hand, the observed WEH is present as hydration of near-surface minerals, then these minerals may

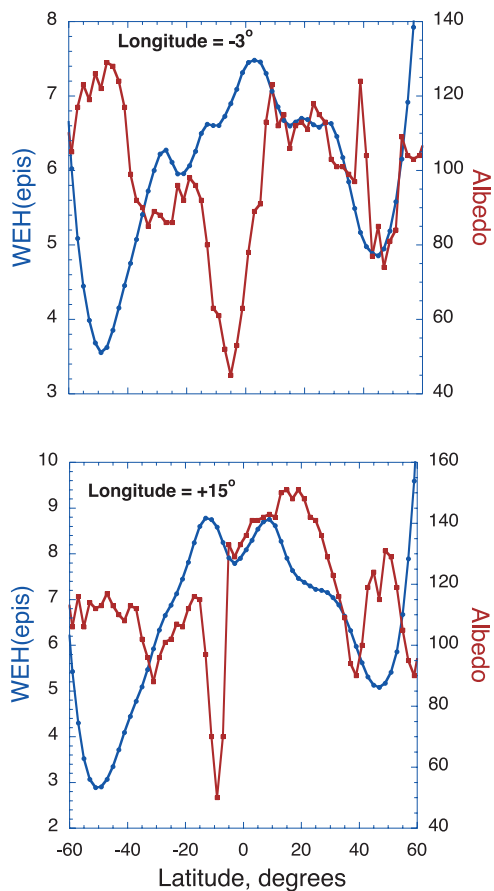


**Figure 2.** Two meridional cuts through the distribution of WEH and albedo that demonstrate the complete lack of correlation between the two.

be stable under present atmospheric conditions [Basilevsky *et al.*, 2003; Bish *et al.*, 2003; Möhlmann, 2004; Feldman *et al.*, 2004b; Vaniman *et al.*, 2004; Fialips *et al.*, 2005]. The lack of a global correlation between WEH abundances and the many surface features that affect WEH stability as water ice [Jakosky *et al.*, 2005], could then be interpreted to infer that the availability of these minerals is spatially variable (i.e., the mineral composition of surface soils on Mars is heterogeneous). It is also possible that the minerals are distributed homogeneously but that the source of WEH is not currently uniformly available; that is, it is determined by factors other than delivery from a static atmosphere under the assumption of a constant water vapor scale height. Another unknown is whether the source of the observed WEH distribution is delivered to the surface from the atmosphere or from a widely distributed, but perhaps non-global water table and water ice reservoir within the cryosphere.

[9] In summary, neither the mechanism of deposition nor the molecular association of water within near-surface regolith at low latitudes to midlatitudes of Mars, are known. The distribution of hydrogen observed from orbit using neutron spectroscopy, parameterized as water-equivalent hydrogen, WEH, could be in the form of inter-pore adsorbates, water ice deposits, and hydrous minerals. We have no reason to believe that a single

mechanism can globally explain the observed water distributions in the Martian near surface regolith. Nevertheless, some mechanisms may operate on much larger scales than others. Whereas a water table and/or water-charged cryosphere can resupply some, but not all locales, the atmosphere can resupply the whole planet. Also, while water-rich salt hydrates, particularly epsomite and hexahydrite, can account for the WEH in Arabia and its antipode near Medusae Fossae [Feldman *et al.*, 2004b], these minerals may not be uniformly distributed because there are some locations where epsomite is inferred to be stable but these regions do not exhibit substantial WEH abundances [Feldman *et al.*, 2004b; Fialips *et al.*, 2005]. Conversely, although epsomite could possibly account for all the WEH observed in the most abundant low-latitude reservoirs, this does not eliminate potential contributions from other hydrous minerals such as zeolites and clays [Bish *et al.*, 2003; Möhlmann, 2004; Vaniman *et al.*, 2004; Fialips *et al.*, 2005].

[10] We also do not know whether the pattern of WEH was emplaced during a recent ice age [Mustard *et al.*, 2001; Christensen, 2003; Head *et al.*, 2003; Mischna *et al.*, 2003; Mischna and Richardson, 2005; Richardson *et al.*, 2002; Mellon and Jakosky, 1993, 1995; Jakosky *et al.*, 1993, 1995], is a residual reservoir from former, more extreme ice ages (extending back to 5 to 10 Ma when obliquities were, at times, greater than  $45^\circ$  [Laskar *et al.*, 2002]), is a consequence of very recent changes in the thickness of the  $\text{CO}_2$  veneer that covers the south residual polar water ice cap [Jakosky *et al.*, 2005], or is in equilibrium with the observed present climate of Mars.

[11] In order to gain insight, we start by trying to establish a timescale for the observed deposits. We then look for regional correlations with surface and atmospheric properties that may be able to discriminate between, or at least provide direction to determine, the potential delivery of water from the atmosphere or from a putative subsurface water reservoir. We will find that although we do not have sufficient experimental knowledge of surface and atmospheric properties to develop a comprehensive, quantitatively credible model, the correlations that are found favor a molecular association with hydratable minerals that are recharged from the atmosphere. We suggest that this delivery path is controlled by local nighttime thermodynamics of the atmosphere (which near the surface is governed by thermal inertia) and the topography of Mars under its present-day orbital state. This state is given by the obliquity, eccentricity, and phase of perihelion relative to the spin axis orientation of Mars. Specifically, the correlations that are found suggest that the spatially dependent atmospheric water convergence provided by the thermally direct north-south Hadley circulation produces surface precipitation of ice within the observed WEH enhanced regions. The presence of this condensed water near and upon the surface raises soil humidity and provides a hydration mechanism for subsurface regolith pores and hydratable minerals. Retention of water of hydration by these minerals will then be favored during the winter months in each hemisphere when the nights are longer and colder, and the slant angle of the Sun during daylight hours is greater, thereby

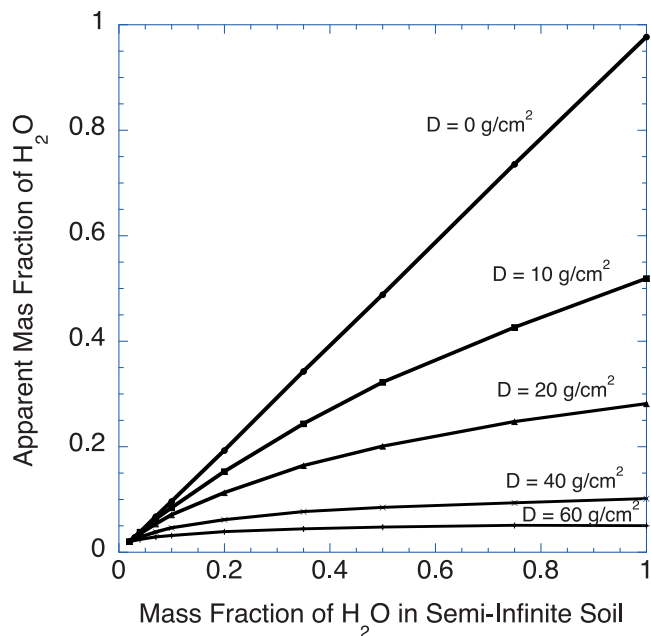


**Figure 3.** Relation between apparent mass fraction of H<sub>2</sub>O calculated from measured epithermal neutron counting rates given by *Feldman et al.* [2004a, equation (1)] and the mass fraction of H<sub>2</sub>O in an assumed semi-infinite model of Martian soil.

yielding longer shadows produced by rough surface terrain.

## 2. Analysis

### 2.1. Timescale

[12] In order to assess the viability of one recharge mechanism over others, we first try to bound the timescale for delivery of water to the surface. The result of this delivery then appears from orbit as the WEH deposits observed using orbital neutron spectroscopy. The largest such deposit near the equator occurs in Arabia, which contains an apparent WEH abundance that ranges between 5% and 10% by mass over an area having diameter of about 2700 km. A simple two-layered model of WEH stratigraphy can be used to show that the dominant deposit of WEH here, must approach within about 60 g/cm<sup>2</sup> (or 40 cm at a density of 1.5 g/cm<sup>3</sup>) of the surface to appear from orbit as having an abundance greater than 5%. The model chosen for this demonstration contains a layer of thickness,  $D$ , of relatively dry soil containing 2% by mass WEH, above a semi-infinite layer of soil with a mass fraction of WEH ranging from 0 to 1 (presented in Figure 3). Inspection shows that to appear as a single semi-infinite deposit of more than 5% WEH by mass, the actual semi-infinite layer, even at 100% WEH, must be closer than 60 g/cm<sup>2</sup> (or 40 cm at a density of 1.5 g/cm<sup>3</sup>) to the surface.

[13] Previous investigations predict the surface dust blanket continuously builds over Arabia at a rate that exceeds, on average, 1  $\mu$ m per year [*Christensen, 1986; Haberle et al., 2003; Basu et al., 2004; Newman et al., 2005*]. If correct, the observed WEH deposit within Arabia must recharge on a timescale that is less than 0.4 Ma. This

conclusion rests on the assumption that dust continues to be available for lifting elsewhere for deposition in Arabia during this time period. However, the mechanisms for net deposition and/or removal of dust from any locale on Mars are still under active study and no consensus has been reached by the planetary community. For example, recent atmospheric numerical modeling with the NASA Ames Mars General Circulation Model (MGCM) suggests that the Arabia region could potentially be a marginal net surface dust deflation region (M. Kahre et al., Modeling the Martian dust cycle and surface dust reservoirs with the NASA Ames general circulation model, submitted to *Journal of Geophysical Research*, 2005). This net deflation is the result of dust devil surface dust lifting (parameterized within the model using the scheme of *Newman et al.* [2002]), which “strips away” accumulating dust deposited from lifting occurring at other geographic locations. The net Arabian surface dust loss in the simulations is only  $\sim 1 \mu$ m per Martian year, very close to zero net gain or loss of dust. Combining these new results with those referenced previously [*Christensen, 1986; Haberle et al., 2003; Basu et al., 2004; Newman et al., 2005*] we can only conclude that the net change in dust cover in Arabia is equal to zero  $\sim \pm 1 \mu$ m per year.

[14] Regardless of any net change in dust cover, we can estimate the time required to evaporate an initially ice-saturated regolith pore volume that may have been charged during a previous, more hydrated Martian climate. Assuming a WEH-filled 40% pore volume and a regolith grain density of 2.7 g/cm<sup>3</sup> yields a mass fraction of WEH of 18.5 mass percent. At an average temperature of 220 K, the top surface of such an initially, fully charged regolith will drop at the rate,

$$dT/dD = 0.178 D^2 \quad (1)$$

where  $T$  is the time in Martian years and  $D$  is the depth to the top surface of the ice table in cm (from *Mellon et al.* [2004, Figure 5]). From Figure 3, such a deposit will appear from orbit to contain less than 5% WEH when  $D$  exceeds 32 cm (assuming a regolith density of 1.5 g/cm<sup>3</sup>). The resultant time required for such a drop is given by  $(0.178/3) D^3 = 1943$  Martian years (or 3655 Earth years). Also from *Mellon et al.* [2004, Figure 5], this time increases to  $1.5 \times 10^4$  Earth years if the average surface temperature is 210 K.

[15] A lower limit to the timescale for WEH recharge can be estimated using the occurrence rates and locations of dust storms. The locations of local and regional dust storms observed using the Mars Orbital Camera (MOC) [*Malin and Edgett, 2001*] between March and December 1999 [*Cantor et al., 2001*] are overlain on a map of WEH in Figure 4. The circles represent the areal extent and locations of the storms, and the distribution of WEH is mapped using a logarithmic scale showing high abundance in blue and low abundance in brown. The two curved white lines that bracket the near-equatorial region mark the 10% WEH contour. Inspection shows that these regional dust storms annually recur at middle latitudes (30° to 60°) in both hemispheres. These zones are observed to occur within regions of relatively low WEH abundances. The timescale for WEH recharge must therefore be longer than several years, otherwise these zones would appear more hydrated.

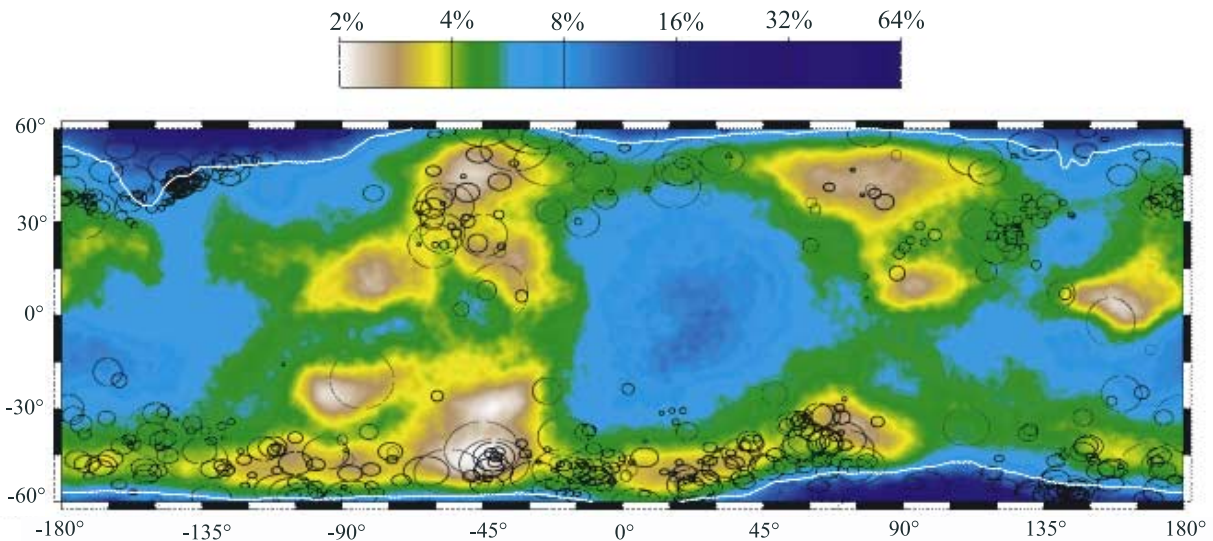


**Figure 4.** Map of the location of regional dust storms. The color scale of WEH is logarithmic extending from 2% (white) to 64% (deep purple). The areal extent of the circles is given at the bottom scale with the areas of the individual regional dust storms.

[16] In summary, our present knowledge of dust deposition and removal on Mars is sufficiently uncertain that we cannot rule out the need for a time-dependent, climate-driven mechanism for the observed equatorial WEH distribution [Jakosky *et al.*, 2005]. Neither can we rule out a mechanism that is consistent with the present-day climate of Mars. We will explore this last possibility in the rest of this paper.

## 2.2. Atmospheric Recharge

[17] We next investigate whether the observed WEH is consistent with recharge from the present-day atmosphere. For this purpose, we compare in Figure 5 the topography of Mars measured using MOLA [Smith *et al.*, 1999], with the abundance of WEH measured using the Mars Odyssey Neutron Spectrometer [Feldman *et al.*, 2004a; Prettyman *et al.*, 2004], and the annually integrated (but not retained) water ice precipitation onto the surface, in  $\text{kg/m}^2$ , simulated using the NASA Ames MGCM (this model is described briefly in Appendix A).

[18] Visual inspection of Figure 5 shows that the observed distribution of WEH does not correlate very well with topography on a global scale, as noted previously [Jakosky *et al.*, 2005]. However, the distribution of WEH outside of Tharsis is in general agreement with the pattern of precipitation of water from the atmosphere to the surface simulated using the MGCM. Note the relatively enhanced water ice deposition over Arabia and the western part of Tharsis, and the relatively low deposition over the two north-south lanes that extend from Acidalia to Argyre on the west of Arabia, and from Utopia through Isidis to Hellas on the east of Arabia. The simulated deposition pattern centered on Arabia is shifted slightly to the north and east relative to the observed WEH peak in the Arabia region. The eastward shift may be related to the slight eastward shift of the Arabia topographic ridge in the

model topography field smoothed to the model's  $5^\circ \times 6^\circ$  spatial resolution.

[19] Although the observed spatial pattern of WEH enhancement was suggested by Jakosky *et al.* [2005] to result from atmospheric deposition, this potential deposition mechanism is modeled here for the first time. We believe that the visually poor correlation between the simulated water ice precipitation over Tharsis (and its volcanic structures) and the observed WEH distribution there does not detract from the successful correlation centered on Arabia. The  $5^\circ \times 6^\circ$  spatial resolution of the model simulation does not readily account for the extreme topographical relief in Tharsis. In particular, none of the Tharsis volcanoes are spatially resolved by the present version of the Ames MGCM grid pattern.

## 2.3. Subsurface Recharge

[20] In order to try to distinguish between an atmospheric source or a subsurface water table source for the observed WEH distribution under present atmospheric conditions, these WEH observations are compared with the topography measured using the Mars Orbiting Laser Altimeter (MOLA) [Smith *et al.*, 1999] in Figure 5. This comparison tests whether topographic features are linked to WEH accumulation at lower latitudes. Specific longitudes of meridional cuts through the WEH distribution and elevation maps shown next, are given by the seven vertical white lines in the WEH map. These meridional cuts are separated into three categories that depend on the possibility of subsurface connectivity to the residual ice cap near the south pole.

[21] Starting first with possible connectivity to the south residual cap through a water table, we explore terrain near Arabia and its antipode using meridional cuts at longitudes of  $179^\circ\text{W}$ ,  $15^\circ\text{E}$ , and  $145^\circ\text{E}$  in Figure 6. Inspection shows that WEH abundances peak near the edge of the high-elevation plateau that overlooks the low-elevation terrain

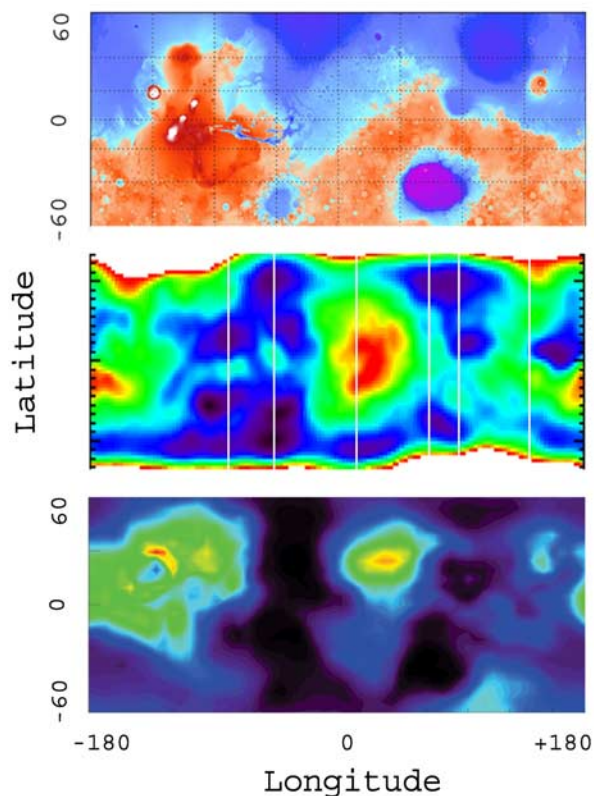


**Figure 5.** Maps of (top) the elevation of the Martian surface, (middle) the WEH abundance (in mass percent), and (bottom) the annual average of water deposited on the surface from the atmosphere simulated using the Ames Mars General Circulation Model. All maps are in cylindrical projection between  $\pm 60^\circ$ . The scale of surface altitude is linear and spans the range from  $-7$  km (purple) to  $21$  km (white). The scale of the WEH abundance is linear and spans between  $2\%$  (purple) and  $10\%$  (red) and that of deposited water is linear and spans from  $0.0$  (deep purple) to  $0.12$  (yellow)  $\text{kg}/\text{m}^2$ .

just north of the plateau at the dichotomy boundary. A secondary peak in the  $145^\circ\text{E}$  longitude cut correlates with the western slope of Elysium Mons. Even more striking is the close correspondence between inflections in the topography and the intermediate peaks and inflections in the  $15^\circ\text{E}$  cut in WEH, both identified by the three vertical black lines.

[22] Other nonmeridional, spherical section cuts that follow the topography more closely, and which better illustrate the correspondence between WEH and topography, are shown in Figure 7. Inspection of track 1, which follows the maximum gradient in topography in Arabia, provides the best example of the relationship between large-scale topographic slope and WEH abundance. However, the correlation between WEH and topography evident in track 2, shown just below track 1, reveals that this relationship is valid only over the central portion of Arabia. Other examples of the close relationship between large-scale topographic slope and WEH content near the dichotomy boundary are also seen in tracks 6 and 0 shown just to the right.

[23] Two meridional cuts that explore the relation between WEH and elevation between about  $50^\circ\text{E}$  and  $100^\circ\text{E}$  longitudes are shown in Figure 8. Here again the correspondence between elevation and WEH abundance is striking. Individual peaks and inflection points in the WEH distribution overlay corresponding peaks and inflection points of the topography for both the  $67^\circ\text{E}$  (Syrtis Major Planum, centered at  $10^\circ\text{N}$ ) and  $85^\circ\text{E}$  (Tyrrhena Terra,

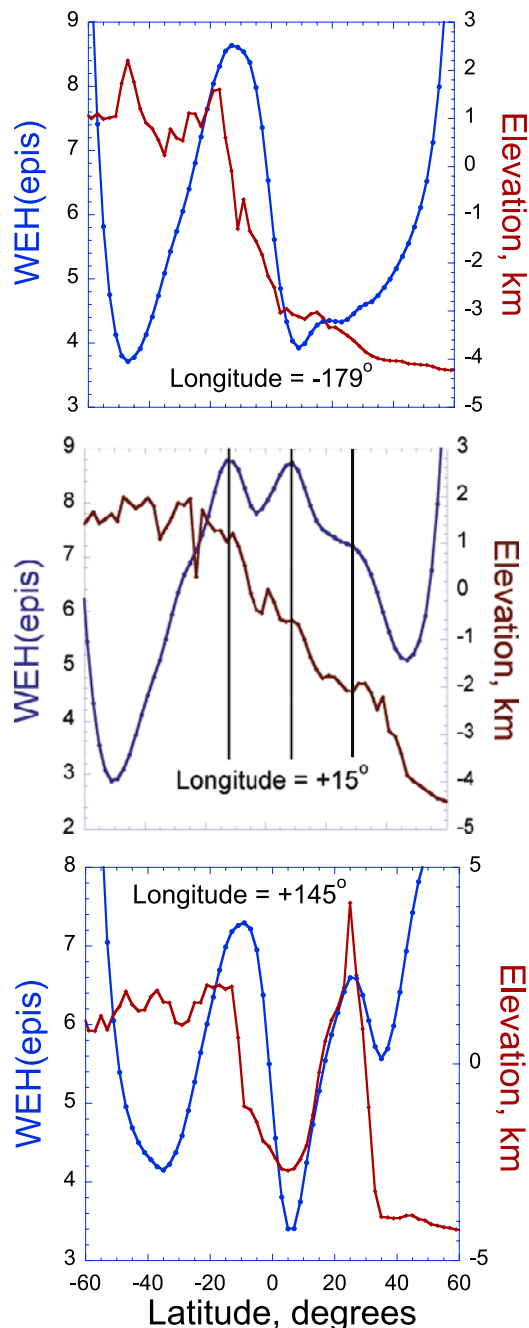


**Figure 6.** Meridional cuts through the topography (red) and WEH abundance (blue) for three longitudes that can potentially connect to the south polar ice cap through the ground. The three black vertical lines locate correlations between inflections and/or relative maxima in the topography and WEH abundance.

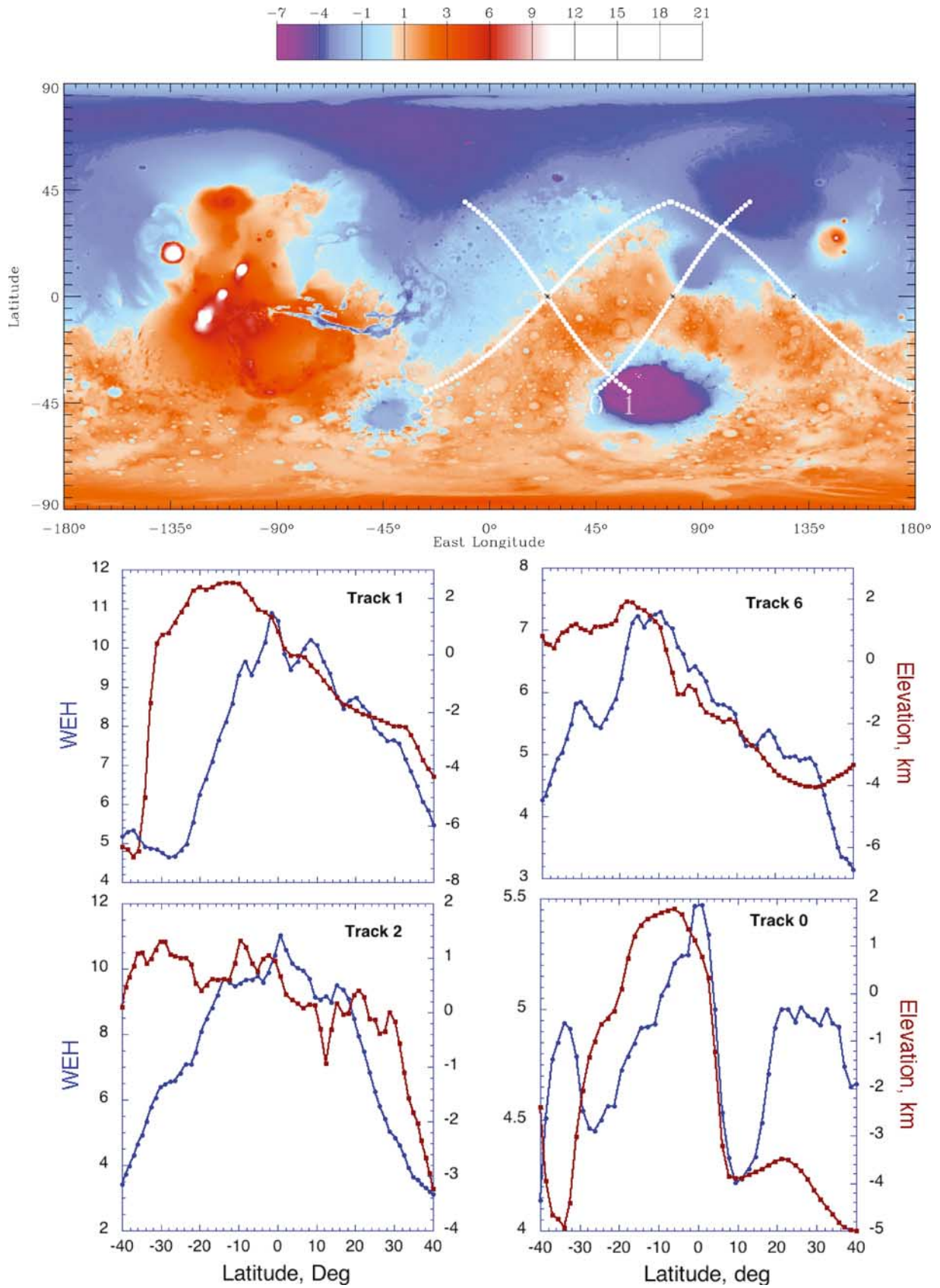
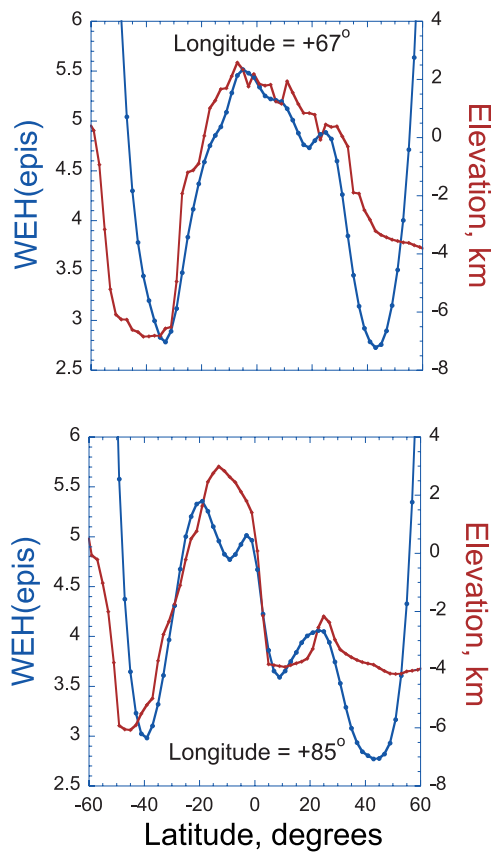


Figure 7



**Figure 8.** Meridional cuts through the topography (red) and WEH abundance (blue) for two longitudes that could possibly connect to the south polar ice cap through the ground but would be significantly impeded by the presence of Hellas just to their south.

peaking at  $10^{\circ}\text{S}$ ) cuts. Furthermore, the topographic rise that separates Isidis from Utopia at  $30^{\circ}\text{N}$  and  $85^{\circ}\text{E}$  also corresponds to a relative maximum in WEH abundance. Both of the foregoing cuts are examples of only marginal possible connectivity to the south residual cap by way of a potential underground water supply. Although it is possible that the WEH here could be supplied through a south cap connecting aquifer, it is unlikely because Hellas Planitia should interpose a significant impediment since its base is almost 8 km below the altitude of neighboring terrain. Likewise, it cannot be supplied from the residual water ice deposit at high northern latitudes through a possible aquifer because the elevation of the north polar ice cap is too low [Zuber *et al.*, 1998]. Another difference between these examples and those shown in Figure 6 is that observed enhancements in WEH shown in Figure 8 occur within low-albedo terrain whereas those in Arabia and near Medusae Fossae have generally high albedo. This example further illustrates the lack of control of WEH by albedo noted earlier.

[24] The last two meridional cuts at  $79^{\circ}\text{W}$  and  $47^{\circ}\text{W}$  in Figure 9, explore the WEH content within the generally dry

terrain between Tharsis and Arabia. Starting first with the  $79^{\circ}\text{W}$  cut, the highest WEH abundance peaks at Tempe Terra ( $40^{\circ}\text{N}$ ), close to the equatorward boundary that separates the stable water ice in the northern reservoir from the unstable, potential midlatitude water ice reservoirs. The next two peaks in WEH abundance straddle the high terrains that form the northern and southern boundaries of Solis Planum. Note that the northernmost peak in WEH occurs north of Valles Marineris (marked by the sharp drop in altitude from +4 km to 0 km from  $5^{\circ}\text{S}$  to  $15^{\circ}\text{S}$ ) and is greater in WEH abundance than the peak that straddles the cordillera that forms the southern boundary of Solis Planum, at  $35^{\circ}\text{S}$ . A similar picture emerges from the meridional cut at  $47^{\circ}\text{W}$ . Here again, the maximum in WEH occurs north of Valles Marineris near the edge of a plateau that overlooks the low-lying terrain north of the dichotomy boundary at about  $5^{\circ}\text{N}$ . None of the peaks in WEH evident in Figure 9 occur in places that can be supplied by the south residual ice cap through an aquifer because they are either too high in altitude or are cut off from the southern cap by deep boundary canyons. Again, there can be no resupply from the north residual polar cap through an aquifer [Zuber *et al.*, 1998].

### 3. Discussion

[25] The primary near-surface WEH reservoirs on Mars reside at high latitudes in both hemispheres. The north reservoir dominates atmospheric resupply at present because the north residual ice cap is relatively large and exposed, and the southern cap is relatively small and covered by a veneer of  $\text{CO}_2$  ice. Such conditions likely did not prevail at earlier times (before about 0.5 Ma ago [Laskar *et al.*, 2002]) when the obliquity of Mars was above  $35^{\circ}$  [Jakosky *et al.*, 1993, 1995; Mellon and Jakosky, 1993, 1995; Mischna *et al.*, 2003], and may not even have been true several hundreds of years ago if the southern cap ever lost its  $\text{CO}_2$  veneer [Jakosky *et al.*, 2005]. Nevertheless, the yearly averaged hemispheric atmospheric water vapor content is considerably higher in the north than in the south [Smith, 2002, 2004]. A greater subtropical concentration of water ice in the form of clouds also appears in the north [Clancy *et al.*, 1996; Smith *et al.*, 2001] during northern summer. At this season, the Hadley cell's ascending branch is located in the vicinity of the subsolar latitude,  $\sim 25^{\circ}\text{N}$ . In the upper branch of this circulation, air flows southward across the equator to a descending zone in the southern subtropics. Surface flow from the descending zone northward across the equator to the ascending zone completes the circulation. As a parcel of atmosphere ascends in the north, its temperature declines as a result of adiabatic expansion. If the water vapor content is great enough and/or the adiabatic cooling sufficient, condensation of water vapor to form ice cloud particles is possible [Clancy *et al.*, 1996; Richardson *et al.*, 2002] at the lifting condensation level (LCL). Since ice cloud particles possess a finite sedimentation speed, which increase with height, ice particles can get "left

**Figure 7.** (bottom) Spherical section cuts through the topography (red) and WEH abundance (blue) along four tracks shown by the white dots in (top) map of MOLA topography. These tracks were chosen to parallel, or run perpendicular to, the large-scale gradient in topography.

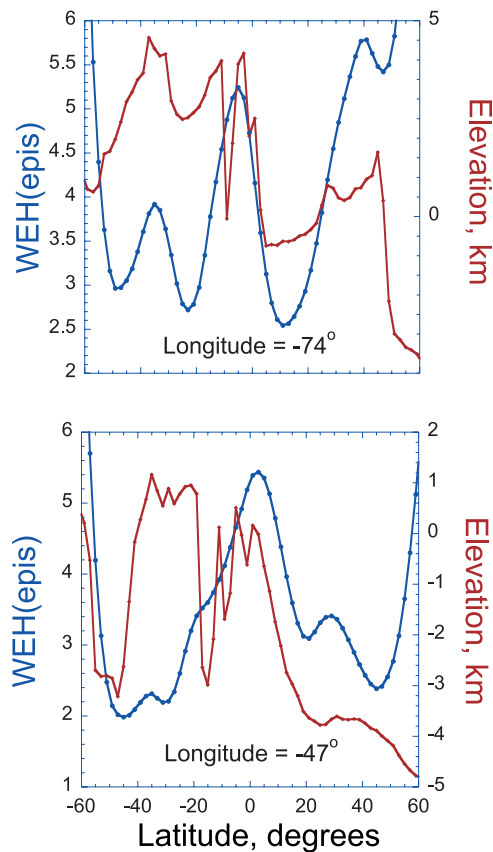


**Figure 9.** Meridional cuts through the topography (red) and WEH abundance (blue) for two longitudes that cannot connect to the south polar ice cap through the ground because they are both at high altitude and are cut off by boundary canyons within the Valles Marineris complex.

behind” in this aphelion cloud belt [Clancy *et al.*, 1996] as their parent air parcel continues to ascend. In this way, desiccated air is transported equatorward in the Hadley cell’s upper branch and then downward within the cell’s descending branch at southern subtropical latitudes. The return northward surface atmospheric flow at low altitudes from the southern region of descent is then relatively dry. This northward surface flow is significantly channeled into longitudinally confined boundary currents that hug the eastern borders of the high Tharsis and Arabia plateaus [Joshi *et al.*, 1995, 1997], potentially desiccating the surface materials within the two longitudinal corridors centered roughly upon the meridian connecting Argyre, Chryse and Acidalia Planitia (at roughly 45°W) east of Tharsis, and Isidis and Utopia Planitia (at roughly 90°E) east of Arabia. Inspection of the middle plot of Figure 5 shows that both of these lanes are indeed relatively desiccated, in agreement with the predicted behavior.

[26] The retention of water in the form of cloud particles within the aphelion cloud belt and the additional water vapor arriving in this region from the exposed north residual cap source increase the water abundance at northern subtropical latitudes during northern summer. This enhanced water abundance, the vertical trapping of the water vapor by cloud formation [Montmessin *et al.*, 2004], and the relatively

cold nighttime surface temperatures over higher terrain with its generally lower thermal inertia, result in preferential near-surface water condensation and precipitation to the surface in the Arabia and Tharsis longitude corridors. This near surface condensation and precipitation extends from 45°N to 45°S at longitudes centered upon 18°E and also upon ~120°W during this northern summer season.

[27] Hinson and Wilson [2004] demonstrated the importance of topography in facilitating water ice precipitation in the regions of Tharsis and Arabia. Using MGS radio occultation measurements collected during  $L_s = 134^\circ - 162^\circ$ , Hinson and Wilson [2004] found nighttime midaltitude (0.3–2 mbar) temperature inversions to be largest and most frequent above elevated terrain such as that at Tharsis and Arabia. Thermal tides are responsible for the temperature inversions. These inversions occur at longitudes of enhanced tidal amplitude, with Tharsis causing the strongest enhancement. Most intriguing is that a prominent cloud layer develops at the base of these inversions where the temperature is a minimum, and a ground fog forms at the surface underneath these inversions in the regions of Tharsis and Arabia [Hinson and Wilson, 2004].

[28] Northern winter water ice precipitation upon the surface within the northern subtropical regions of observed equatorial WEH enhancement is also produced within the Ames MGCM simulation. The observed (and MGCM simulated) enhanced northern subtropical atmospheric water vapor abundance during northern winter arises because of the transport of water from southern latitudes without a confining perihelion cloud belt desiccating the transported air. This northern subtropical precipitation is again longitudinally confined to the Arabia and Tharsis regions. These longitudinal regions correspond to the regions experiencing the coldest nighttime surface temperatures, which would therefore be the regions most likely to experience condensation (for uniform water vapor mixing ratio). Thus the equatorial and subtropical longitude corridors observed to possess enhanced WEH coincide with the regions at which the Ames MGCM predicts near-surface water condensation and surface ice accumulation (at least at night with subsequent daytime sublimation) under current climatic conditions. The simulated presence of nighttime water upon the surface occurs throughout the year north of the equator and is confined to winter south of the equator.

[29] Another point of agreement between present atmospheric conditions and observed low-latitude to midlatitude WEH abundances is that the steep slopes of the topographic dichotomy boundary are preferentially hydrated. The northernmost ridges of the highlands terrain are observed to have the highest hydration state (see Figures 6–9). Preliminary results using the Ames MGCM indicate these locations as maximum deposition regions and that bulk deposition maximizes near in time to the solstices. Near the solstices in the daytime, equatorial near surface winds are from the winter to the summer hemisphere. At night, near surface winds decouple from the larger-scale atmospheric flow. Air in contact with the surface cools via conduction and radiation and flows down the slope of the local topography. During southern summer, this flow is opposite the direction of the large-scale thermally direct circulation. The near-surface cooled air possesses water vapor, and at locations where the temperature is below the condensation temperature

(which depends on the relative humidity), precipitation occurs. The coldest near-surface temperatures occur at the locations of lowest thermal inertia (which generally correspond to the longitudes of highest surface elevation within this latitude zone), and thus a wave number two pattern of water deposition (precipitation) occurs at Tharsis and Arabia. The simulated water deposition pattern is shown in the bottom plot of Figure 5. Comparison with the observed map of WEH just above it shows a similarity of hydration patterns, although there are differences in detail. Both have a wave number two longitudinal pattern, with relative maxima in the vicinity of topographic ridges. Relative minima follow the lanes of low-topographic desiccation centered on Acidalia, Chryse, and Argyre in the west, and Utopia, Isidis, and Hellas in the east.

[30] Episodic surface water ice within the regions of inferred enhanced WEH abundance need not be a net water source for hydratable minerals under current conditions. Rather, the ice presence could act as a “governor” minimizing the loss rate of WEH emplaced there previously under different climatic conditions. In this scenario, the observed WEH maxima regions are experiencing a net loss of WEH, with this desiccation having the longest timescale at those locations (longitudes) at which water condenses upon the surface under current climate conditions. This presumes, but does not require, that surface water was made available under previous climatic conditions at all or multiple longitudes within the latitude range spanned by the detected equatorial WEH maxima.

[31] Relatively dry and strong winds also occur during spring in both hemispheres along the periphery of their retreating seasonal CO<sub>2</sub> frost cover at high latitudes. This condition is evidenced by the occurrence of local dust storms there. A comparison of the locations of dust storms observed during parts of 1999 [Cantor *et al.*, 2001] relative to observed WEH abundances is shown in Figure 4. It is seen that these storms generally follow east-west lanes of relatively desiccated terrain between about 30° and 60° from the equator in both hemispheres. This pattern also agrees with present atmospheric conditions on Mars. The dust storm tracks also match the locations of disaggregated terrain, explained [Mustard *et al.*, 2001; Milliken *et al.*, 2003] as the desiccated remains of formerly ice-rich subsurface deposits.

[32] The possibility of a subsurface metastable water ice deposit fed by diffusion of water vapor from a groundwater system may be inferred from the models developed by Mellon *et al.* [1997]. Such a subsurface deposit cannot be observed from orbit using neutron spectroscopy because predicted deposit depths exceed 4 m everywhere at low latitudes to midlatitudes. However, shallow deposits of hydrous minerals supported by the resultant upward diffusion of water molecules from such subsurface water ice deposits could be possible. We believe this possibility is unlikely. If a global water table exists on Mars, as suggested by Clifford and Parker [2001], it should be most visible north of the dichotomy boundary where the depth to water or water ice should be least. This condition is not observed. WEH abundances are much lower within Isidis, Utopia, and Acidalia than they are in Arabia and its antipode near Medusae Fossae, both of which are south of the dichotomy boundary [Feldman *et al.*, 2004a]. In addition, if the

enhanced WEH deposits lying just north of Valles Marineris shown in Figure 9 are caused by a water table fed from the residual south polar water ice deposit, it should show up more prominently in the highland terrain just south of Valles Marineris, which is contrary to observations.

#### 4. Conclusions

[33] At present, we cannot discern the hydration mechanism for the observed longitudinally constrained distribution of equatorial WEH. However, our study suggests that the current epoch of Martian climate history can sustain, if not emplace, the observed equatorial WEH distribution. The correspondence between relative maxima in WEH abundances with maximum occurrence of north facing topographic slopes at low latitudes to midlatitudes of Mars suggest that the locations of low thermal inertia, high topography, and accompanying low near-surface temperatures couple with the large-scale atmospheric circulation patterns to control the deposition onto, and/or vapor diffusion into, surface soils from the atmosphere. Once within the soils, the WEH can be retained by hydrating minerals that are present and stable under local subsurface conditions [Feldman *et al.*, 2004b; Fialips *et al.*, 2005]. The general concentration of atmospheric water vapor is observed to occur north of the equator [Smith, 2002], which is not consistent with the observed distribution of near-surface WEH. In contrast, the WEH distribution is concentrated on the north facing slopes of the dichotomy boundary as well as on the highest terrain in the southern highlands. This pattern is consistent with simulations using the Ames MGCM, which predict a wave number two longitudinal pattern of equatorial and subtropical water ice precipitation on Mars, with relative precipitation maxima in the vicinity of Arabia and Tharsis. Relative minima of simulated precipitation follow the observed desiccated upper regolith lanes of Acidalia, Chryse, and Argyre in the west, and Utopia, Isidis, and Hellas in the east. Precipitation occurs mainly at night in locations where the temperature is below the local condensation temperature. These coldest temperatures occur at longitudes of lowest thermal inertia and highest topography. The nighttime deposition of water ice upon the surface (followed by sublimation after sunrise) occurs throughout the year north of the equator. Here, the vertical trapping of the water by the aphelion cloud belt in the summer and the enhanced northern subtropical water vapor abundance during northern winter produce a nearly year-round supply of condensable water vapor. Nighttime water ice deposition is constrained to winter south of the equator. There is no perihelion cloud belt to confine water vapor to the southern hemisphere during summer, and the warmer perihelion temperatures rarely fall below the condensation temperature at night. So the only condensable water vapor is during winter when nighttime temperatures dip below the dew point and condensable water is provided by the cross-equatorial portion of the Hadley circulation.

[34] We note though, that the presence of condensable water or precipitated water ice is not by itself sufficient to account for the observed spatial distribution of WEH. Retention of these surface water deposits by hydratable minerals depends on the subsurface distribution of these minerals (which is not presently known) as well as the water

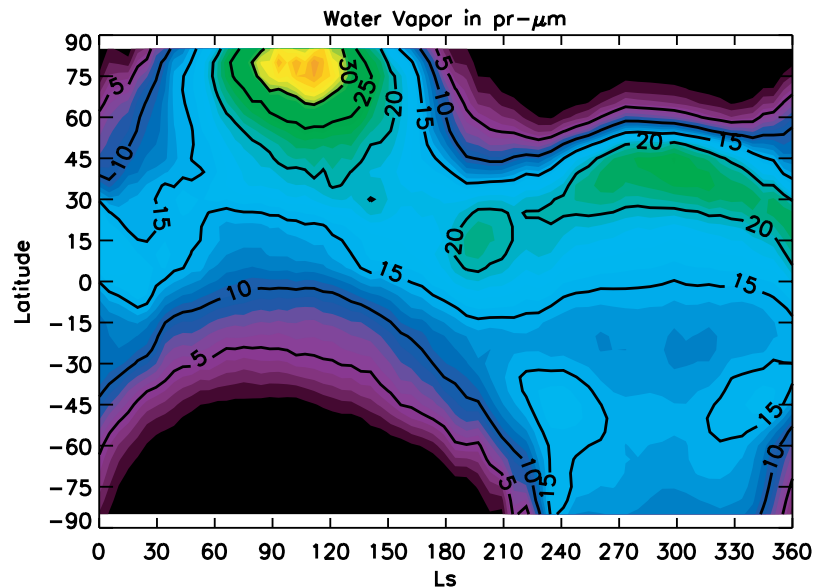


**Figure A1.** Simulated atmospheric water vapor abundance for one Mars year in precipitable micrometers.

deposition patterns that occur during the winter months. During these times, the nights are longer and colder, and the daytime shadows cast by irregular surface terrain are longer, thereby reducing the loss rate of recently deposited water back to the atmosphere.

[35] Although water ice is nowhere stable equatorward of  $\pm 30^\circ$  [Farmer and Doms, 1979; Paige, 1992; Jakosky and Haberle, 1992; Mellon and Jakosky, 1993], making it less likely that observed WEH abundances result from atmospheric or subsurface circulation-replenished water ice deposits, many different hydrous minerals could be at least partially hydrated throughout this region [Bish *et al.*, 2003; Möhlmann, 2004; Feldman *et al.*, 2004b; Vaniman *et al.*, 2004; Fialips *et al.*, 2005]. In addition, the hydration states of these minerals are sensitive to atmospheric wind speed and relative humidity. Quantitative calculations using potential hydrous minerals in surface soils show that no one mineral family can explain all WEH observations at low latitudes to midlatitudes of Mars, suggesting the presence of a heterogeneous mixture of hydrous minerals [Feldman *et al.*, 2004b; Fialips *et al.*, 2005]. A hydrous mineral interpretation of observed WEH deposits is also favored by the lack of correlation between albedo and WEH. If the WEH were indeed the water ice remnants from a previous hydrated atmosphere phase, then its evaporation rate should be highest where albedo is lowest and the average subsurface temperature is correspondingly highest. This expectation is not met, as shown in Figure 2.

## Appendix A: Global Circulation Model Description

[36] The NASA Ames Mars GCM (Version 2.0) is a finite difference numerical grid point model of the Martian atmosphere with a heritage dating back to terrestrial atmosphere modeling in the 1960s [Leovy and Mintz, 1969]. Currently implemented model processes include (1) treatment of radiative transfer in the visible and infrared for gas

and dust [Toon *et al.*, 1989], (2)  $\text{CO}_2$  condensation and sublimation [Haberle *et al.*, 1999], (3) spatially variable MOLA surface topography [Smith *et al.*, 1999] and thermal inertia and albedo fields (based on Viking and Mars Global Surveyor observations (F. Forget, personal communication, 2005)), (4) explicit boundary layer treatment [Haberle *et al.*, 1993, 1999], (5) surface stress [Newman *et al.*, 2005; Haberle *et al.*, 2003] and dust devil-dependent dust lifting [Newman *et al.*, 2002] and particle size-dependent dust sedimentation, and (5) water sublimation, transport, condensation to ice cloud particles, and sedimentation and sublimation of these cloud particles. The model's dynamical core (including tracer transport) solves the atmospheric thermodynamic equations on a  $5^\circ$  latitude  $\times$   $6^\circ$  longitude Arakawa C grid [Suarez and Takacs, 1995].

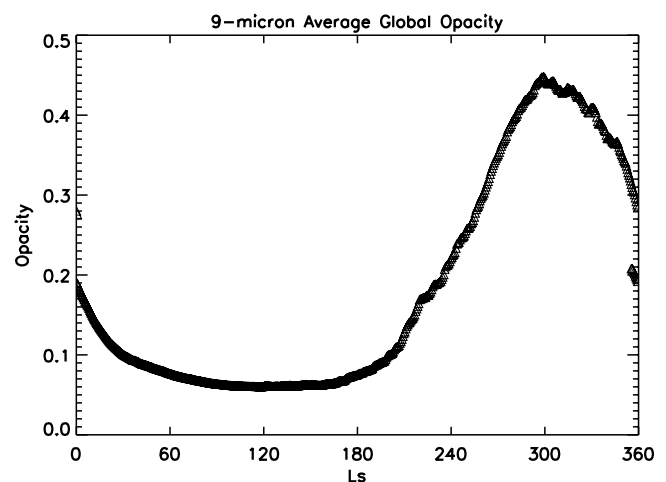


**Figure A2.** Simulated 9 micron average global opacity as a function of time of year, given by areocentric longitude,  $L_s$ .

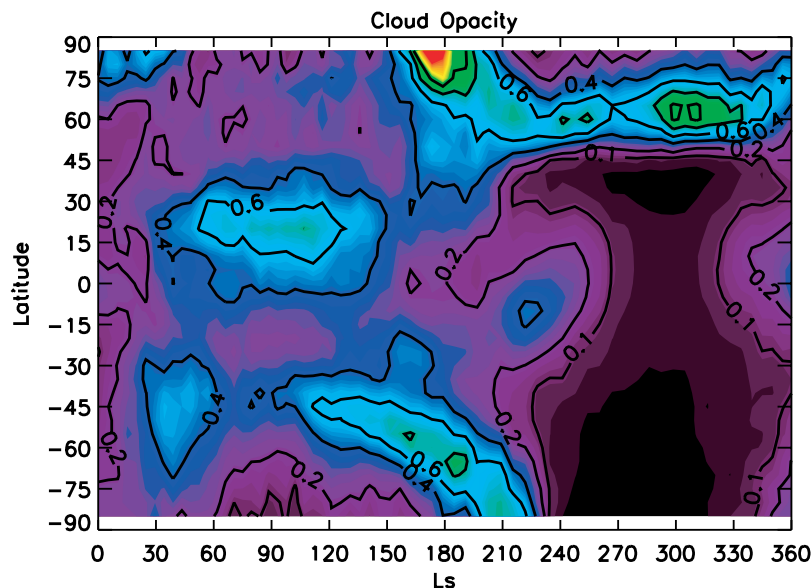


**Figure A3.** Zonally averaged cloud opacity as a function of time of year, given by areocentric longitude,  $L_s$ .

[37] Lifted dust particles are  $1.5 \mu\text{m}$  in radius [Wolff and Clancy, 2003], possess a density of  $2500 \text{ kg/m}^3$ , and experience gravitational sedimentation. The suspended dust opacity is employed for radiative heating consideration within the correlated  $k$  radiative transfer routine covering 12 spectral bands tailored for the Mars  $\text{CO}_2$ /water vapor atmosphere covering the range of 0.3 to 250 microns (R. Haberle, personal communication, 2005). Visible dust opacity in the model is twice the infrared value [Martin, 1986; Clancy et al., 2003].

[38] A surface water ice source (albedo = 0.5, thermal inertia =  $2000 \text{ J m}^{-2} \text{ s}^{-1/2} \text{ K}^{-1}$ ) is seasonally exposed at the most northerly model latitude ( $85^\circ\text{N}$ ). The water sublimation rate from this ice cap is calculated via the wind and humidity-dependent prescription of Haberle and Jakosky [1990]. Water (cloud particle) condensation is controlled by the saturation vapor pressure and is condensation nuclei (dust particle abundance) limited. When local saturation is exceeded, 90% of the local dust particles are available to serve as cloud particle condensation nuclei, however, dust is not removed from the atmosphere to form the resulting cloud particles. Resultant ice cloud particles are assumed to possess a  $4 \mu\text{m}$  radius [Wolff and Clancy, 2003; Clancy et al., 2003] and a density that accounts for both the water ice and presumed dust content. Excess condensable water (for which nuclei are not available) is carried as supersaturated vapor. If cloud particles pass through a subsaturated region during horizontal advection or vertical sedimentation (or ascent), cloud particles are sublimed until saturation is reached or all cloud particles are sublimed. Water deposition upon the surface occurs because of sedimentation of cloud particles (no surface frost occurs), with sedimentation speed based on the Stokes-Cunningham flow for a spherical particle [Pruppacher and Klett, 2000].

[39] The annual water vapor cycle generated by the model (Figure A1) exhibits the observed seasonality seen by TES [Smith, 2002, 2004], with a north polar maximum abundance ( $\sim 50\%$  of that observed) resulting from exposure of

the north polar ice cap during northern summer. Enhanced column water vapor abundances progress equatorward as northern summer progresses. The observed northern subtropical winter column water vapor content maximum is reproduced by the model, though the simulated abundance is too wet by  $\sim 25\%$ . The observed south polar maximum is also present in the model results, though the simulated abundance is  $\sim 40\%$  of that observed. The simulated globally integrated water abundance is within a few tens of percent of that measured by TES [Smith, 2002], except during northern spring. The minimum value of  $1.5 \times 10^{12} \text{ kg}$  of water vapor during northern spring is  $\sim 50\%$  too high, but the maximum of  $2.3 \times 10^{12} \text{ kg}$  throughout southern spring, is comparable (within  $\sim 10\%$ ) to TES results [Smith, 2002].

[40] The simulated dust (column integrated IR opacity) cycle (Figure A2) within this same simulation mimics the  $9 \mu\text{m}$  globally averaged dust optical depth measured by TES [Smith, 2004], with one exception. The  $\sim 0.4$  opacity peak in the model occurs at  $L_s \sim 300$ ,  $60^\circ$  of  $L_s$  later than that seen in observation. The simulated minimally dusty northern summer season matches TES measurements of a globally averaged minimum opacity of 0.06. This background opacity, the result of the parameterized dust devil lifting, is very critical for the formation of an aphelion cloud belt.

[41] The model produces an aphelion water ice cloud belt between  $30^\circ\text{N}$  and just south of the equator (Figure A3) at an altitude of  $\sim 1$  scale height ( $\sim 10 \text{ km}$ ). This cloud belt extends seasonally from  $L_s \sim 30^\circ$  to  $150^\circ$ , consistent with the seasonal extent as derived from TES spectra [Smith, 2002, 2004]. Polar hood clouds form over the edges of the winter seasonal cap, as observed. The whole of the planet is relatively cloud free during the perihelion season, with the exception of the north polar hood. Simulated maximum cloud opacities (calculated according to Montmessin et al. [2004]) are 3–4 times higher than those derived from TES spectra. Montmessin et al. [2004] suggest that this modeled

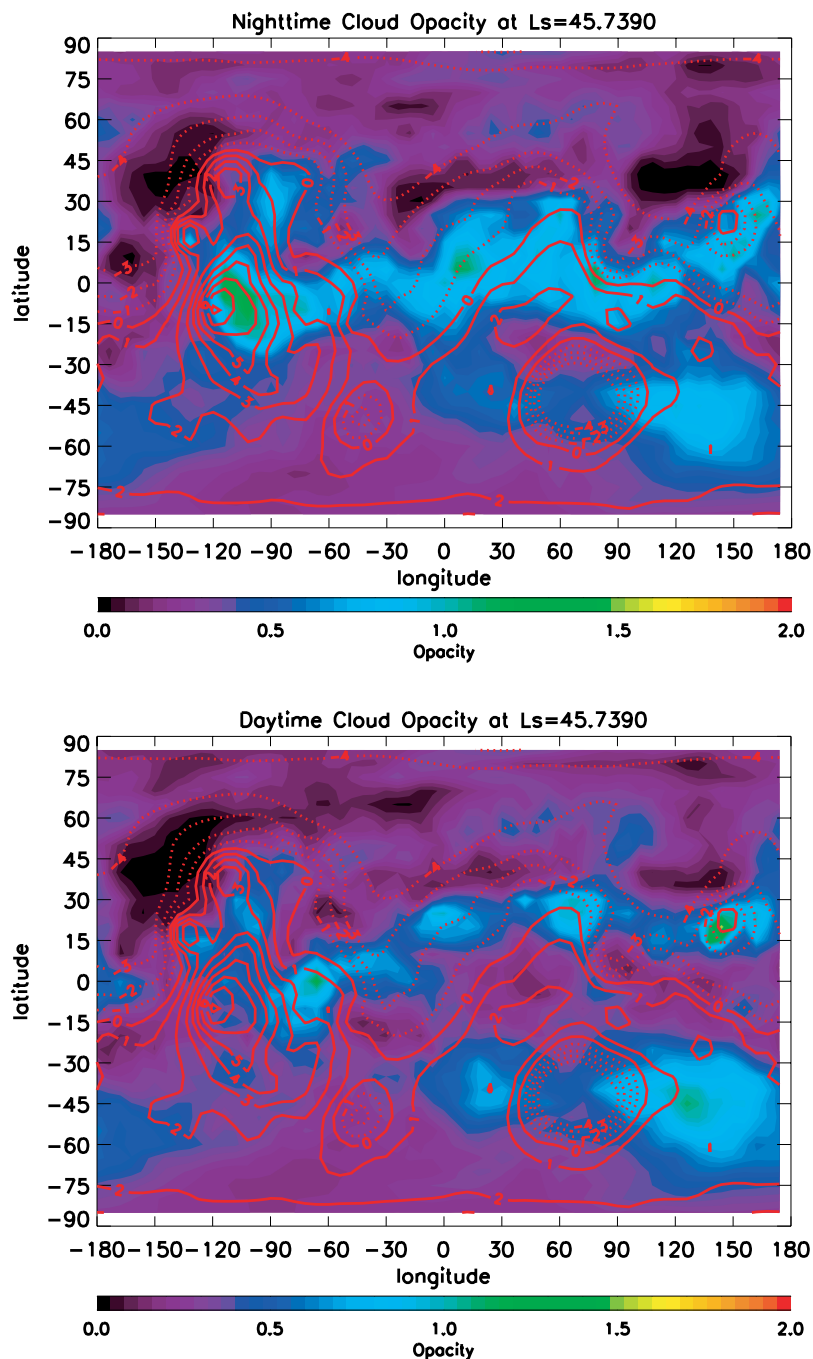


**Figure A4.** (top) Nighttime and (bottom) daytime column-integrated cloud opacity during midnorthern spring.

overestimate can be attributed to the monodisperse particle size employed in this simulation.

[42] Simulated cloud opacity typically decreases from morning to midday (Figure A4). A similar trend is recorded by Viking orbiter camera data [Tamppari *et al.*, 2003] and modeled by Hinson and Wilson [2004]. Similar to the GFDL model results [Hinson and Wilson, 2004], the Ames GCM predicts cloud coverage in the predawn hours to be larger in opacity and spatial extent, with the largest opacities occurring over Tharsis. The premise of the model results for this current paper is the nighttime formation and precipita-

tion of water ice clouds over Tharsis and Arabia in the form of a ground fog generated over these two low thermal inertia regions. Hinson and Wilson [2004] refer to such ground fog formation but no mention is made of the precipitation effects. The simulated nighttime clouds at Tharsis and Arabia that are responsible for the deposition in the Ames GCM are consistent with the wave two pattern of nighttime clouds of Wilson and Smith [2005]. They found that 2 AM TES derived ground temperatures were anomalously warm compared to the GFDL model in the regions of Tharsis and Arabia. Wilson and Smith [2005] concluded that by includ-

ing into their model radiatively active water ice clouds, their model was able to match the spatial extent and amplitude of the observed surface temperature anomaly.

[43] **Acknowledgments.** We wish to thank Bruce Jakosky and John Wilson for their many useful suggestions for improvement of this manuscript. Partial support of this work was provided by the DOE through Laboratory Directed Research and Development funds and by NASA (NASA/NAG5-12123 awarded to New Mexico State University) and was conducted under the auspices of the DOE.

## References

- Basilevsky, A. T., M. L. Litvak, I. G. Mitrofanov, W. V. Boynton, R. S. Saunders, and J. W. Head (2003), Search for traces of chemically bound water in the Martian surface layer based on HEND measurements onboard the 2001 Mars Odyssey spacecraft, *Sol. Syst. Res.*, *37*, 387–396.
- Basu, S., M. I. Richardson, and R. J. Wilson (2004), Simulation of the Martian dust cycle with the GFDL Mars GCM, *J. Geophys. Res.*, *109*, E11006, doi:10.1029/2004JE002243.
- Bish, D. L., J. W. Carey, D. T. Vaniman, and S. J. Chipera (2003), Stability of hydrous minerals on the Martian surface, *Icarus*, *164*, 96–103.
- Boynton, W. V., et al. (2002), Distribution of hydrogen in the near surface of Mars: Evidence for subsurface ice deposits, *Science*, *297*, 81–85.
- Cantor, B. A., P. B. James, M. Caplinger, and M. J. Wolff (2001), Martian dust storms: 1999 Mars Orbiter Camera, *J. Geophys. Res.*, *106*, 23,653–23,687.
- Christensen, P. R. (1986), Regional dust deposits on Mars: Physical properties, age, and history, *J. Geophys. Res.*, *91*, 3533–3545.
- Christensen, P. R. (2003), Formation of recent Martian gullies through melting of extensive water-rich snow deposits, *Nature*, *422*, 45–48.
- Christensen, P. R., et al. (2001), Mars Global Surveyor Thermal Emission Spectrometer experiment: Investigation description and surface science results, *J. Geophys. Res.*, *106*, 23,823–23,871.
- Clancy, R. T., A. W. Grossman, M. J. Wolff, P. B. James, D. J. Rudy, Y. N. Billawala, B. J. Sandor, W. S. Lee, and D. O. Muhleman (1996), Water vapor saturation at low altitudes around Mars aphelion: A key to Mars climate?, *Icarus*, *122*, 36–62.
- Clancy, R. T., M. J. Wolff, and P. R. Christensen (2003), Mars aerosol studies with the MGS TES emission phase function observations: Optical depths, particle sizes, and ice cloud types versus latitude and solar longitude, *J. Geophys. Res.*, *108*(E9), 5098, doi:10.1029/2003JE002058.
- Clifford, S. M. (1998), Mars: The effect of stratigraphic variations in the regolith diffusive properties on the evolution and vertical distribution of equatorial ground ice, *Lunar Planet. Sci. Conf.* [CD-ROM], *XXIX*, abstract 1922.
- Clifford, S. M., and T. J. Parker (2001), The evolution of the Martian hydrosphere: Implications for the fate of a primordial ocean and the current state of the northern plains, *Icarus*, *154*, 40–79.
- Farmer, C. B., and P. E. Doms (1979), Global seasonal variation of water vapor on Mars and the implications of permafrost, *J. Geophys. Res.*, *84*, 2881–2888.
- Feldman, W. C., et al. (2002), Global distribution of neutrons from Mars: Results from Mars Odyssey, *Science*, *297*, 75–78.
- Feldman, W. C., S. Maurice, T. H. Prettyman, M. T. Mellon, S. W. Squyres, S. Karunatillake, R. C. Elphic, H. O. Funsten, D. J. Lawrence, and R. L. Tokar (2003), Association of measured distribution of near-surface hydrogen at high northerly latitudes with surface features on Mars, in *Third International Conference on Mars Polar Science and Exploration* [CD-ROM], abstract 8101, Lunar Planet. Inst., Houston, Tex.
- Feldman, W. C., et al. (2004a), Global distribution of near-surface hydrogen on Mars, *J. Geophys. Res.*, *109*, E09006, doi:10.1029/2003JE002160.
- Feldman, W. C., et al. (2004b), Hydrated states of MgSO<sub>4</sub> at equatorial latitudes on Mars, *Geophys. Res. Lett.*, *31*, L16702, doi:10.1029/2004GL020181.
- Feldman, W. C., J. W. Head, S. Maurice, T. H. Prettyman, R. C. Elphic, H. O. Funsten, D. J. Lawrence, R. L. Tokar, and D. T. Vaniman (2004c), Recharge mechanism of near-equatorial hydrogen on Mars: Atmospheric redistribution or sub-surface aquifer, *Geophys. Res. Lett.*, *31*, L18701, doi:10.1029/2004GL020661.
- Fialips, C. I., J. W. Carey, D. T. Vaniman, W. C. Feldman, and M. T. Mellon (2005), Hydration state of zeolites, clays, and hydrated salts under present-day Martian surface conditions: Can hydrous minerals account for Mars Odyssey observations of near-equatorial water-equivalent hydrogen?, *Icarus*, in press.
- Haberle, R., and B. Jakosky (1990), Sublimation and transport of water from the north residual polar cap on Mars, *J. Geophys. Res.*, *95*, 1423–1437.
- Haberle, et al. (1993), A boundary-layer model for Mars: Comparison with Viking Lander and entry data, *J. Atmos. Sci.*, *50*, 1544–1559.
- Haberle, R. M., M. M. Joshi, J. R. Murphy, J. R. Barnes, J. T. Schofield, G. Wilson, M. Lopez-Valverde, J. L. Hollingsworth, A. F. C. Bridger, and J. Schaeffer (1999), General circulation model simulations of the Mars Pathfinder atmospheric structure investigation/meteorology data, *J. Geophys. Res.*, *104*, 8957–8974.
- Haberle, R. M., J. R. Murphy, and J. Schaeffer (2003), Orbital change experiments with a Mars general circulation model, *Icarus*, *161*, 66–89.
- Head, J. W., J. F. Mustard, M. A. Kreslavsky, R. E. Milliken, and D. R. Marchant (2003), Recent ice ages on Mars, *Nature*, *426*, 797–802.
- Hinson, D. P., and R. J. Wilson (2004), Temperature inversions, thermal tides, and water ice clouds in the Martian tropics, *J. Geophys. Res.*, *109*, E01002, doi:10.1029/2003JE002129.
- Jakosky, B. M., and R. M. Haberle (1992), The seasonal behavior of water on Mars, in *Mars*, edited by H. H. Kieffer et al., pp. 969–1016, Univ. of Ariz. Press, Tucson.
- Jakosky, B. M., B. G. Henderson, and M. T. Mellon (1993), The Mars water cycle at other epochs: Recent history of the polar caps and layered terrain, *Icarus*, *102*, 286–297.
- Jakosky, B. M., B. G. Henderson, and M. T. Mellon (1995), Chaotic obliquity and the nature of the Martian climate, *J. Geophys. Res.*, *100*, 1579–1584.
- Jakosky, B. M., M. T. Mellon, E. S. Varnes, W. C. Feldman, W. V. Boynton, and R. M. Haberle (2005), Mars low-latitude neutron distribution: Possible remnant near-surface water ice and a mechanism for its recent emplacement, *Icarus*, *176*, 12–43.
- Joshi, M. M., S. R. Lewis, P. L. Read, and D. C. Catling (1995), Western boundary currents in the Martian atmosphere: Numerical simulations and observational evidence, *J. Geophys. Res.*, *100*, 5485–5500.
- Joshi, M. M., R. M. Haberle, J. R. Barnes, J. R. Murphy, and J. Schaeffer (1997), Low-level jets in the NASA Ames Mars general circulation model, *J. Geophys. Res.*, *102*, 6511–6524.
- Laskar, J., B. Levrard, and J. F. Mustard (2002), Orbital forcing of the Martian polar layered deposit, *Nature*, *419*, 375–377.
- Leovy, C., and Y. Mintz (1969), Numerical simulation of the atmospheric circulation and climate of Mars, *J. Atmos. Sci.*, *26*, 1167–1190.
- Malin, M. C., and K. S. Edgett (2001), Mars Global Surveyor Mars Orbiter Camera: Interplanetary cruise through primary mission, *J. Geophys. Res.*, *106*, 23,429–23,570.
- Martin, T. Z. (1986), Thermal infrared opacity of the Mars atmosphere, *Icarus*, *66*, 2–21.
- Mellon, M. T., and B. M. Jakosky (1993), Geographic variations in the thermal and diffusive stability of ground ice on Mars, *J. Geophys. Res.*, *98*, 3345–3364.
- Mellon, M. T., and B. M. Jakosky (1995), The distribution and behavior of Martian ground ice during past and present epochs, *J. Geophys. Res.*, *100*, 11,781–11,799.
- Mellon, M. T., B. M. Jakosky, and S. E. Postawko (1997), The persistence of equatorial ground ice on Mars, *J. Geophys. Res.*, *102*, 19,357–19,369.
- Mellon, M. T., K. A. Kretke, M. D. Smith, and S. M. Pelkey (2002), A global map of thermal inertia from Mars Global Surveyor mapping mission data, *Lunar Planet. Sci.* [CD-ROM], *XXXIII*, abstract 1416.
- Mellon, M. T., W. C. Feldman, and T. H. Prettyman (2004), The presence and stability of ground ice in the southern hemisphere of Mars, *Icarus*, *169*, 324–340.
- Milliken, R. E., J. F. Mustard, and D. L. Goldsby (2003), Viscous flow features on the surface of Mars: Observations from high-resolution Mars Orbiter Camera (MOC) images, *J. Geophys. Res.*, *108*(E6), 5057, doi:10.1029/2002JE002005.
- Mischna, M. A., and M. I. Richardson (2005), A reanalysis of water abundances in the Martian atmosphere at high obliquity, *Geophys. Res. Lett.*, *32*, L03201, doi:10.1029/2004GL021865.
- Mischna, M. A., M. I. Richardson, R. J. Wilson, and D. J. McCleese (2003), On the orbital forcing of Martian water and CO<sub>2</sub> cycles: A general circulation model study with simplified volatile schemes, *J. Geophys. Res.*, *108*(E6), 5062, doi:10.1029/2003JE002051.
- Mitrofanov, I., et al. (2002), Maps of subsurface hydrogen from the High Energy Neutron Detector, Mars Odyssey, *Science*, *297*, 78–81.
- Möhlmann, D. T. F. (2004), Water in the upper Martian surface at mid and low latitude: Presence, state, and consequences, *Icarus*, *168*, 318–323.
- Montmessin, F., F. Forget, P. Rannou, M. Cabane, and R. M. Haberle (2004), Origin and role of water ice clouds in the Martian water cycle as inferred from a general circulation model, *J. Geophys. Res.*, *109*, E10004, doi:10.1029/2004JE002284.
- Mustard, J. F., C. D. Cooper, and M. K. Rifkin (2001), Evidence for recent climate change on Mars from the identification of youthful near-surface ground ice, *Nature*, *412*, 411–414.

- Newman, C. E., S. R. Lewis, P. L. Read, and F. Forget (2002), Modeling the Martian dust cycle, 1. Representations of dust transport processes, *J. Geophys. Res.*, *107*(E12), 5123, doi:10.1029/2002JE001910.
- Newman, C. E., S. R. Lewis, and P. L. Read (2005), The atmospheric circulation and dust activity in different orbital epochs on Mars, *Icarus*, *174*, 135–160.
- Paige, D. A. (1992), The thermal stability of near-surface ground ice on Mars, *Nature*, *356*, 43–45.
- Prettyman, T. H., et al. (2004), Composition and structure of the Martian surface at high southern latitudes from neutron spectroscopy, *J. Geophys. Res.*, *109*, E05001, doi:10.1029/2003JE002139.
- Pruppacher, H. R., and J. D. Klett (2000), *Microphysics of Clouds and Precipitation*, 416 pp., Springer, New York.
- Richardson, M. I., R. J. Wilson, and A. V. Rodin (2002), Water ice clouds in the Martian atmosphere: General circulation model experiments with a simple cloud scheme, *J. Geophys. Res.*, *107*(E9), 5064, doi:10.1029/2001JE001804.
- Richardson, M. I., D. J. McCleese, M. Mischna, and A. R. Vasavada (2003), Obliquity, ice sheets, and layered sediments on Mars: What spacecraft observations and climate models are telling us, *Lunar Planet. Sci.* [CD-ROM], *XXXIV*, abstract 1281.
- Smith, D. E., et al. (1999), The global topography of Mars and implications for surface evolution, *Science*, *284*, 1495–1507.
- Smith, M. D. (2002), The annual cycle of water vapor on Mars as observed by the Thermal Emission Spectrometer, *J. Geophys. Res.*, *107*(E11), 5115, doi:10.1029/2001JE001522.
- Smith, M. D. (2004), Interannual variability in TES atmospheric observations of Mars during 1999–2003, *Icarus*, *167*, 148–165.
- Smith, M. D., J. C. Pearl, B. J. Conrath, and P. R. Christensen (2001), Thermal Emission Spectrometer results: Mars atmospheric thermal structure and aerosol distribution, *J. Geophys. Res.*, *106*, 23,929–23,945.
- Suarez, M. J., and L. L. Takacs (1995), Technical report series on global modeling and data assimilation, vol. 5, Documentation of the AIRES/GEOS dynamical core, version 2, *NASA Tech. Memo. 104606*, NASA, Greenbelt, Md.
- Tamppari, L. K., R. W. Zurek, and D. A. Paige (2003), Viking-era diurnal water-ice clouds, *J. Geophys. Res.*, *108*(E7), 5073, doi:10.1029/2002JE001911.
- Tokar, R. L., W. C. Feldman, T. H. Prettyman, K. R. Moore, D. J. Lawrence, R. C. Elphic, M. A. Kreslavsky, J. W. Head III, J. F. Mustard, and W. V. Boynton (2002), Ice concentration and distribution near the south pole of Mars: Synthesis of odyssey and global surveyor analyses, *Geophys. Res. Lett.*, *29*(19), 1904, doi:10.1029/2002GL015691.
- Toon, O. B., C. P. McKay, T. P. Ackerman, and K. Santhanam (1989), Rapid calculation of radiative heating rates and photodissociation rates in inhomogeneous multiple scattering atmospheres, *J. Geophys. Res.*, *94*, 16,287–16,301.
- Wilson, R. J., and M. D. Smith (2005), The effects of atmospheric opacity on the seasonal variation of Martian surface temperature, *Lunar Planet. Sci. Conf.* [CD-ROM], *XXXVI*, abstract 1947.
- Wolff, M. J., and T. Clancy (2003), Constraints on the size of Martian aerosols from Thermal Emission Spectrometer observations, *J. Geophys. Res.*, *108*(E9), 5097, doi:10.1029/2003JE002057.
- Vaniman, D. T., D. L. Bish, S. J. Chipera, C. I. Fialips, J. W. Carey, and W. C. Feldman (2004), Magnesium sulphate salts and the history of water on Mars, *Nature*, *431*, 663–665.
- Zuber, M. T., et al. (1998), Observations of the north polar region of Mars from the Mars Orbiter Laser Altimeter, *Science*, *282*, 2053–2060.

---

R. Elphic, W. C. Feldman, H. O. Funsten, D. J. Lawrence, T. H. Prettyman, R. L. Tokar, and D. T. Vaniman, Los Alamos National Laboratory, Los Alamos, NM 87545, USA. (wfeldman@lanl.gov)  
 O. Gasnault and S. Maurice, Centre d'Etude Spatiale des Rayonnements, Toulouse F-31400, France.  
 J. R. Murphy and S. Nelli, Department of Astronomy, New Mexico State University, Las Cruces, NM 88003, USA.